DOE-EPSCoR: Exchange interactions in epitaxial intermetallic layered systems

Award # DE-FG02-08ER46499

PI: Patrick R. LeClair, The University of Alabama

1 Accomplishments

1.1 Magnetic transition behavior in Fe-Rh-Pd films deposited at various substrate temperatures

1.1.1 Background

Fe-Rh has attracted much interest due to its wide range of magnetic properties. It exhibits a first order magnetic transition around 400 K from ferromagnetism ($T > 400$ K) to antiferromagnetism[1,2] ($T < 400$ K). This transition temperature can be tuned by adding a third element to the compound. For example, the addition of Ni and Pd decreases the transition temperature, whereas the addition of Pt and Ir increases it.[3–5] The transition temperature can be also tuned by changing the sputtering conditions,[6] which suggests a sensitivity of the magnetic transition to structural parameters. Since Fe-Rh alloys have a transition from antiferromagnetism to ferromagnetism near room temperature, they could have potential technological applications (e.g., heat assisted magnetic recording[7–9]). However, the fundamental factors governing the phase transition behavior have not been completely elucidated. In particular, the structural and magnetic properties of thin films with thickness of less than 50 nm have not been reported. Prior studies focus on relatively thick films with annealing treatments at high temperature (up to 800°C) after deposition[10] or bulk samples.[3–5] Generally, a large strain could be induced in thinner films, which could yield distinctly different magnetic properties. Therefore, from a fundamental point of view, it is very important to study the magnetic properties of Fe-Rh and Fe-Rh-M films with thicknesses in the range where significant strain could be induced. Moreover, since these materials could be employed in magnetic recording media with typical thicknesses of less than 20 nm, understanding the relationship between strain and magnetic properties is paramount. In this study, the magnetic and structural properties of 30 nm thick Fe-Rh-Pd films were examined in order to elucidate the influence of induced strain to film on the Fe-Rh-Pd magnetic properties.

1.1.2 Results

All Fe-Rh-Pd films were fabricated by a homemade ultra high vacuum magnetron sputtering system with a background pressure of less than 9×10^{-7} Pa. Films of Fe-Rh-Pd were directly deposited on MgO(001) substrates from a composite $Fe_{47}Rh_{47}Pd_6$ target. The layers were capped with a 3 nm thick Pt layer in order to avoid natural oxidization. The growth temperature, T_g was varied from 400°C to 700°C. The structural properties were characterized by high angle X-ray diffraction. The magnetic properties were evaluated using a superconducting quantum interference device (SQUID; Quantum Design MPMS).

Figure 1 shows XRD patterns for Fe-Rh-Pd films grown at T_g from 400°C to 700°C . All films showed only [001] planes oriented normal to the film plane, and Fe-Rh-Pd[001] superstructure diffraction peaks can be clearly observed in all films which indicates that the ordered B2 structure is present. The epitaxial growth of Fe-Rh-Pd layers on MgO(001) substrates was confirmed by measuring the out-of plane diffraction peaks. The out of plane diffraction results indicate that

the Fe-Rh-Pd[100] axis was rotated by 45° with respect to the MgO[100] axis, as generally can be observed in bcc films deposited on MgO(001) substrates.

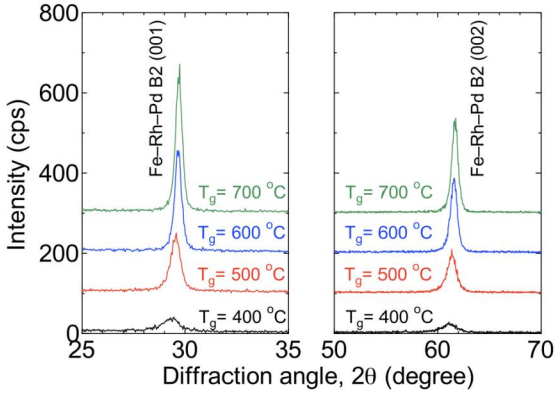

Figure 1: XRD patterns for FeRhPd films deposited on MgO(001) substrates with increasing growth temperature. Curves are vertically offset for clarity.

Since the magnetic transition of this material can only be observed in the B2 (ordered) phase, it is necessary to evaluate the chemical order parameter, S, in these films. The integral intensity ratios of (001) diffraction peaks to (002) diffraction peaks, I_{001}/I_{002}, were calculated in order to evaluate the values of S, since the ratio I_{001}/I_{002} is proportional to the square of the order parameter.[11] A calculated result for the integral intensity ratio is shown as a function of T_g in Fig. 2. The integral intensity ratio, I_{001}/I_{002}, is almost independent of the growth temperature which indicates that the growth temperature had no significant influence on the degree of chemical ordering in this growth temperature range. On the other hand, the lattice constants do change as the growth temperature is increased, as shown in Fig. 2. In order to obtain accurate lattice constant values for Fe-Rh-Pd films, Cohens method was used.[12,13] The (001), (002), (101), and (112) lattice spacing values were measured by XRD, and subsequently those lattice spacing values were related with a linear function in accordance with Cohens method, along with the appropriate error function.[14] Although bulk Fe-Rh-Pd with B2 structure is a cubic structure, the film is treated as a tetragonal structure, since the lattice constants along the direction perpendicular to the films' planes may be different from that along the lateral direction, due to the epitaxial mismatch between the Fe-Rh-Pd layer and MgO substrate. The lattice constant along the film normal (c) decreased with increasing growth temperature, whereas the lattice constant along the lateral directions (a) increased. This can be explained by a mismatch between the Fe-Rh-Pd equilibrium lattice and the MgO substrate lattice. Since MgO has smaller lattice spacing along the lateral directions, it is expected that a compressive stress should cause a contraction of the lattice along the lateral (a) directions while the value of the perpendicular lattice constant (c) should increase to maintain a constant lattice volume. The compressive strain is relaxed as the growth temperature increases, since the lattice constant values are observed to converge toward their equilibrium values as the growth temperature increases. This change in crystal structure affects the magnetic transition behavior significantly.

Figure 2 shows the magnetic transition curves for the fabricated Fe-Rh-Pd films with decreasing measurement temperature. No magnetic field was applied during the measurement of the magnetic transition. The films fabricated from 500°C to 700°C showed an almost complete magnetic transition, whereas the Fe-Rh-Pd film fabricated at 400°C showed only a partial transition with a large residual ferromagnetic moment even at low temperature. This distinct change in the transition temperature with increasing the growth temperature could be attributed to the structural change

with increasing the growth temperature. The transition curves were fitted by a simple linear function near the center of transition (50% transition), and the transition temperatures were defined as the temperatures where slopes in the fitted curves showed maximum values. Transition widths were defined as temperature ranges where the magnetization values changed from 90% to 10% between maximum and minimum magnetization values.

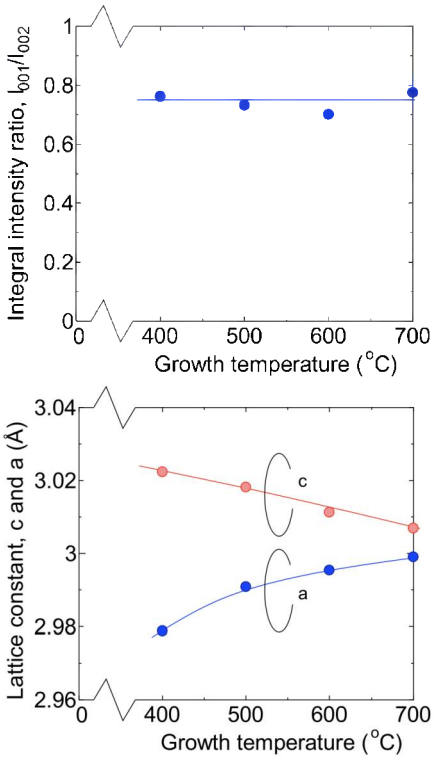

Figure 2: **(left)** The integral intensity ratio, I_{001}/I_{002}, as a function of the growth temperature. **(right)** Values of the lattice constants of c and a for Fe-Rh-Pd films deposited on MgO(001) substrates as a function of the growth temperature.

Figure 3 shows the transition temperature dependence of the growth temperature. The transition temperature monotonically decreased as the growth temperature increased. This is in sharp contrast to the case of FeRh films on MgO(100), where it was reported that the magnetic transition temperature increased as the annealing temperature is increased.[6] The difference between these two experimental results is that the Fe-Rh-Pd films grown at different temperatures show a change of lattice constant values with an almost constant lattice volume (about 0.8% increase in lattice volume with increasing the growth temperature), whereas both lattice constant values along perpendicular direction and lateral direction decreased as the annealing temperature increased in Fe-Rh binary alloy films[6]. The lattice volume should be important parameter in this transition behavior because this magnetic transition is driven by a magneto-volume instability, and is accompanied by a distinct change in the lattice volume.[8,15,16]

A relatively large transition slope was observed in the Fe-Rh-Pd films in present study compared to that observed in other studies.[3–5] This is probably because of residual structural inhomogeneities in the films. Since there is some mismatch between the Fe-Rh-Pd layers and MgO substrates, mismatch strain, plane dislocations and/or anti phase boundaries are formed. These structural dislocations should increase the slope of the magnetic transition curve. The transition width (ΔT_g), which is related to the slope of the transition curve, is shown in Table **??**. The transition width increased with increasing the growth temperature, which may suggest that structural or compositional inhomogeneity increased with increasing the growth temperature. It seems most likely that the inhomogeneity is in the lateral directions, since the out of plane XRD peaks narrow as growth temperature increases, suggesting less inhomogeneity along the perpendicular direction. On the other hand, the Fe-Rh-Pd fabricated at 400°C with annealing treatment after the deposition showed steep slope in transition curve.[17] Since the annealing treatment should have the effect of reducing structural inhomogeneity, this result supports our speculation regarding the transition behavior.

From a technological point of view, importantly, the transition temperature could be tuned by

T_g (°C)	ΔT_g (°C)
500	72
600	90
700	104

inducing strain in the fabricated films. The transition temperature of the Fe-Rh in heat assisted magnetic recording media should be optimized so that the dynamic coercivity of the media at the highest temperature can be suppressed well below the limited writing field available. Further tuning of the strain may be accomplished by applying appropriate seed of buffer layers to the fabrication method.

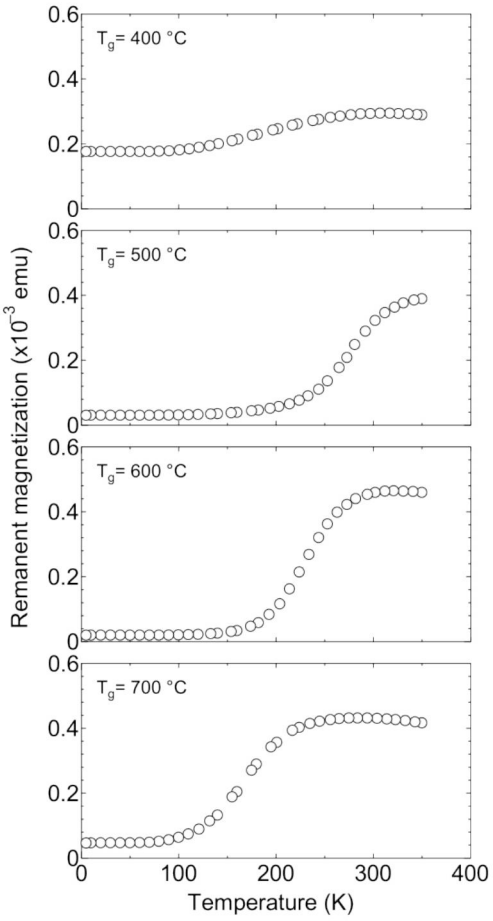

Figure 3: Temperature dependence of remanent magnetization as a function of measurement temperature. No magnetic field was applied during measurement.

In summary, Fe-Rh-Pd films were fabricated on MgO(001) substrates. The fabricated films exhibit a reduction in the transition temperature with an increase in the growth temperature, which can be attributed to changes in the crystal structure. These results show an apparent

opposite tendency to the experimental results in Fe-Rh binary alloy films, however differences could be attributed to differences in processing. Significant property variation may be achieved through high temperature deposition as compared to post-deposition annealing.

1.2 Inelastic Neutron Scattering from Dy/Y Superlattices

1.2.1 Background

Inelastic neutron scattering is one of the most powerful tool to study the magnetic excitations of solids. To date, a spin wave dispersion relation in an antiferromagnetic thin film has yet to be measured. The primary reasons involve insufficient neutron flux and analyzer sensitivity (leading to prohibitively long acquisition times on equipment that is very expensive to operate), and a lack of longer wavelength neutrons to more effectively probe the larger magnetic unit cell. Recent upgrades at the High Flux Isotope Reactor (HFIR) neutron scattering facility have led to dramatic improvements in usable neutron flux coupled with lower background signals. When sufficiently high quality samples are realized, a primary goal will be to measure the spin wave dispersions in a layered material to demonstrate that spin wave quantization occurs in structures with at least one dimension approaching the atomic scale. For accomplishing this task, a set of Dy/Y superlattices of around 250 total bi-layers were fabricated at MINT center, University of Alabama. The designed period of the superlattices and the epitaxial structure of the multilayers were verified by the X-ray diffraction and pole figure measurements. The neutron diffraction and inelastic neutron scattering performed at Oak Ridge National Laboratory further confirmed the quality of the samples.

1.2.2 Results

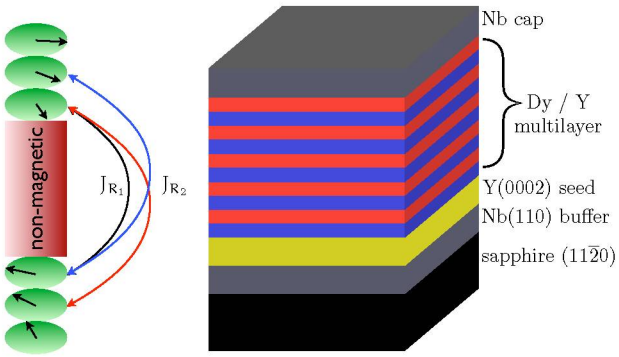

Figure 4: Schematics of the helical Dy moments (left) [5] and the Dy/Y superlattice (right) [2]. The spin wave excitations in Dy will be confined within the layers and coupled weakly by indirect exchange.

Dysprosium was chosen for its large local magnetic moment ($10.6\,\mu_B$), which gives greater magnetic scattering strength. Yttrium was selected in order to match the lattice structure and spacing of Dysprosium. Previous research has shown that Y grows epitaxially on the Nb[110] surface, and Nb[110] single crystalline films can be grown on $Al_2O_3[11\bar{2}0]$ substrates [18]. Thus, the multilayer structures were designed as shown in Fig. 4 (right) [19]. On a $Al_2O_3[11\bar{2}0]$ substrate, a 40 nm Nb[110] buffer layer is grown, which not only avoids an oxidation reaction between sapphire substrate and rare-earth elements, but also seeds the epitaxial growth of the hexagonal close packed (hcp) rare-earth elements. Subsequently, a 20 nm epitaxial Y[0001] seed layer can be grown on the Nb[110] buffer layer, and epitaxial Dy(4.5 nm)/Y(2.9 nm) [0001] bilayers are repeatedly stacked on Y seed

layer. Finally, a 10 nm Nb protecting layer is used in order to protect the highly reactive Dy and Y.

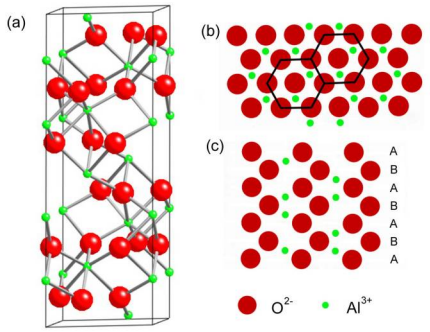

Figure 5: **(a)** Corundum, the structure of Al_2O_3 [10], **(b)** 2-D structure on c-plane (0001) Al_2O_3 [11], **(c)** 2-D structure on a-plane $(11\bar{2}0)$ Al_2O_3.

Dy has the hcp structure, with lattice constants $a = 0.3593$ nm and $c = 0.5655$ nm, and Y, also in the hcp structure, has a 2% lattice mismatch ($a = 0.3650$ nm and $c = 0.5641$ nm). The spacing between the Dy or Y [0002] atom planes is $c/2$, so the 4.5 nm Dy and 2.9 nm Y layers in [0001] orientation comprising the repeating multilayer unit correspond to 16 Dy atomic layers and 10 Y atomic layers. Bulk Dy develops an incommensurate helical magnetic order of the $4f$ spins below the Nèel temperature (178 K),[18] and has a ferromagnetic transition at 85 K induced by a combination of anisotropy and magnetostrictive interactions.[19] Figure 4 (left)[20] shows a schematic of the helical order in Dy. The Dy helix has a period of about 2.3 nm (giving a turn angle per layer of $\Delta\Phi = 46°$) at 165 K, and around 3.4 nm ($\Delta\Phi = 30°$) below 80 K, where bulk Dy would be ferromagnetic in the basal plane.[21] (The Y is non-magnetic at all temperatures.) The helical magnetic order of Dy can be maintained across the intervening Y layers due to the Ruderman-Kittel-Kasuya-Yosida (RKKY) interaction, which provides long range magnetic coherence through nonmagnetic layers.[22–24] The J_{R_i} in Fig. 4 represents the RKKY interactions between Dy layers.

The structure of the Al_2O_3 substrate has the corundum structure, shown in Fig. 5a.[25] The larger O atoms form an hcp structure, and the Al atoms occupy two interstices in the close-packed O atom plane, forming a hexagonal basal plane in the graphite structure.[26] Figure 5 (b) shows a top view of the corundum structure along the c-axis, with one basal plane of the hcp O atoms and hexagonal Al atoms. Figure 5 (c) illustrates the atom arrangement on the surface of a-plane sapphire we used. The Nb buffer layer has bcc structure, and on $Al_2O_3[11\bar{2}0]$ will grow epitaxially in a [110] orientation, which will in turn seed the growth of [0002]-oriented hcp Dy and Y.

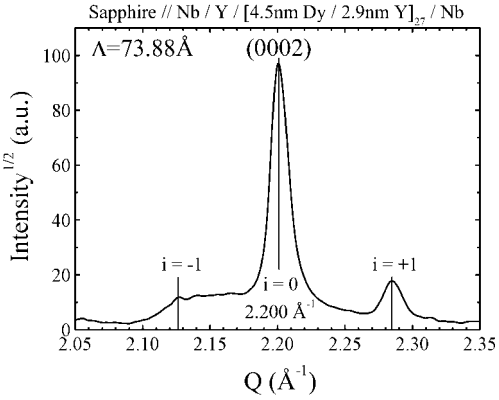

Figure 6: X-ray diffraction of the Dy/Y [0002] diffraction peak for a superlattice with 27 repeats.

A series of $[\mathrm{Dy}(4.5\,\mathrm{nm})/\mathrm{Y}(2.9\,\mathrm{nm})]_n$ ($n = 6, 8, 27, 54, 80$) samples were fabricated by the ADAM sputtering system at a base pressure of $\sim 10^{-9}$ Torr. The ADAM system is equipped with four 1.5 in sputtering guns, two computer-controlled shutters, a temperature controller (up to 900°C), and a sample rotator which improves the uniformity of films on larger substrates. For a 1×1 inch substrate, uniformity could be controlled to within 2% with sample rotation, compared to ~35% without sample rotation. X-ray diffraction was used to characterize the quality and epitaxy of the multilayers, and as expected, clear Bragg peaks from Al_2O_3[11-20], Nb[110], and

Dy/Y[0002] were found in all superlattices. The two satellite peaks around the Dy/Y[0002] main peak in Figure 6 are the feature of periodic multilayer. Although the left satellite is not clear due to the attenuation of the Ni filter used (this is not the reason for the difference), the superlattice period can be calculated by the separation between the main peak at the right satellite. The superlattice period Λ (i.e., the thickness of one Dy/Y bi-layer) as measured from the right satellite agrees with the nominal deposition thicknesses to within 1% of the desired period (4.5+2.9 nm = 7.4 nm).

Pole figure measurements can be used to reveal the epitaxy of the films by elucidating the in-plane symmetries present. In our case, the Dy/Y $[10\bar{1}1]$ plane was examined. From the geometry of the hexagonal lattice and the c/a ratio of the Dy/Y lattice, the Dy/Y $[10\bar{1}1]$ plane is around 61° with respect to the [0001] plane or the film surface. Thus, by setting the angle $\psi = 60°$, the Dy/Y $[10\bar{1}1]$ plane can be aligned perpendicular to the plane of incidence, which is determined by the incident beam and the detector. When fixing 2θ at the diffraction peak of Dy/Y $[10\bar{1}1]$ (around 32.7°), a ψ scan over 360° would give 6 diffraction peaks separated by 60°, reflecting the 6-fold symmetry of the $[10\bar{1}1]$ plane. Figure 7 shows the pole figure peaks as expected, confirming the epitaxy of the multilayer. The [0001] planes of the sapphire substrates were also examined in order to verify the relationship between the substrate and film orientation. The sapphire [0001] plane showed the expected 2-fold symmetry.

X-ray reflectivity was used to further characterize the quality of the superlattices, shown in Fig. 8 For a nanometer-scaled thin film multilayer, the intensity of X-rays reflected from the multilayer may show oscillations, called Kiessig fringes. When a film is grown on a substrate, the interference between the wave reflected by the film surface and the wave reflected at the film-air interface can be either constructive or destructive, and this gives rise to the Kiessig fringes.[27] The intensity decreases rapidly with increasing the angle of incidence; it can be shown that the decay of the reflected X-ray intensity follows a Q^{-4} law[28] (where Q is the momentum transfer) when the angle of incidence is greater than the critical angle, below which the X-rays would be totally reflected. The critical angle is usually defined as the angle of incidence at which the reflected intensity drops to 50% of its maximum value.[29] In perfect superlattices, there should be Bragg peaks at low angles due to the periodicity of the multilayer, and the Kiessig fringes appear as an oscillating background between the peaks. Figure 8 shows the X-ray reflectivity results for our sample, where the intensity has been multiplied by Q^4 in order to compensate for the Q^{-4} decay. The Bragg peaks can be observed up to the second order, indicating that we indeed have a regular superlattice, consistent with the x-ray diffraction results presented above. Due to the presence of some surface roughness, the reflected intensities of the

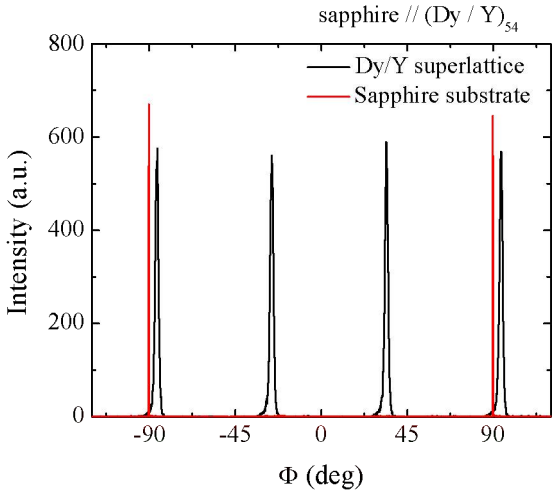

Figure 7: Pole figure measurement for Dy/Y $[10\bar{1}1]$ plane and sapphire [0001] plane.

first and second Bragg peaks only a fraction of the peak corresponding to the total reflection, and the Kiessig fringes between the Bragg peaks are relatively weak. The superlattice period can be evaluated by the separation of the Bragg peaks and the critical angles, and the calculated bi-layer thickness is within 10% of the expected values.

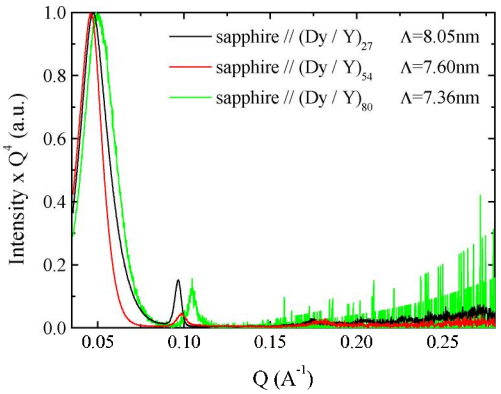

Figure 8: Normalized intensity (intensity $\times$ Q^4) versus Q for the Dy/Y superlattices with different numbers of repeats.

The XRD and XRR results confirmed the expected quality of the superlattices, of sufficient quality for initial neutron diffraction measurements. The neutron scattering measurements are performed at HFIR, High Flux Isotope Reactor, located in Oak Ridge National Laboratory, by our collaborator Dr. J. Lee Robertson. Our initial neutron diffraction measurements yielded magnetic superlattice peaks due to the helical magnetic ordering in Dy, shown in Fig. 9 for the Dy (002) diffraction peaks. The magnetic superlattice peaks develop below $\sim 165\,\mathrm{K}$, the bulk magnetic ordering temperature of Dy, and confirm that a magnetic periodicity exists within the sample below that temperature. Further, the magnetic superlattice period deduced from the satellite peaks agrees well with both the nominal deposition thicknesses and the superlattice period deduced from X-ray diffraction measurements. Figure 9 also shows the inelastic neutron diffraction results, which are a first indication for quantized magnetic excitations in this system resulting from confinement. Further experiments, currently underway, will improve the signal to noise ratio in the inelastic experiment by using larger samples with more repetitions. We will also investigate a wider range of multilayers with various Dy atomic layers to further evaluate the RKKY interactions as a function of Dy and Y layer spacing.

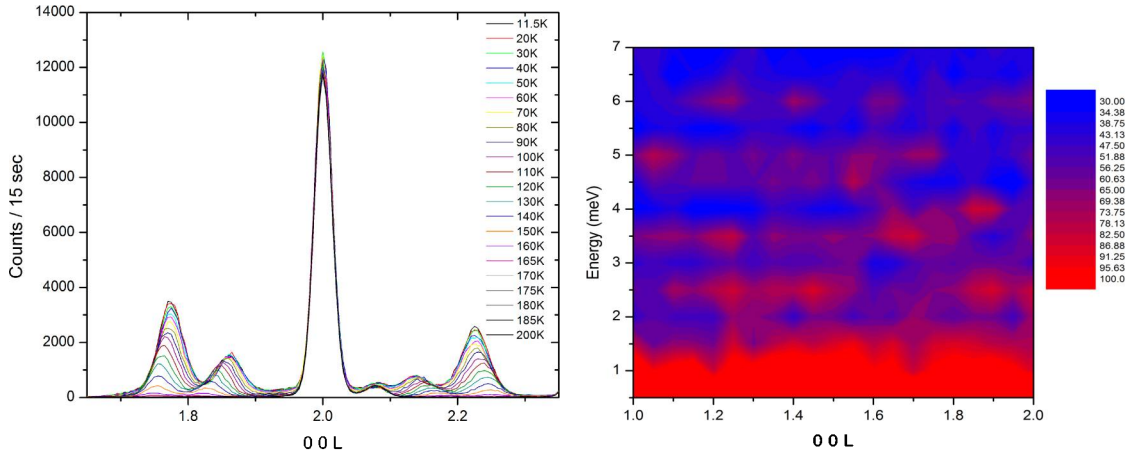

Figure 9: **(left)** Magnetic satellite peaks due to helical magnetic ordering in Dy as a function of the temperature. **(right)** Inelastic neutron diffraction results showing quantized excitations due to confinement.

1.3 Polarized Neutron Reflectometry of FePtRh heterostructures

1.3.1 Background

FePt-based alloys are typically the material of choice for magnetic information storage media. The high magnetic moment of Fe gives a large magnetization, while the large atomic number of Pt results in a high magnetic anisotropy. This combination of high magnetization and high anisotropy enables written bits to be smaller than ever before, since magnetic grains with a high magnetic anisotropy are more thermally stable. Another desirable feature is that the anisotropy often results in perpendicular magnetization (relative to the film plane), which is the preferred orientation for current media. Although these materials are widely used, our fundamental understanding of the fundamental physics governing the behavior of magnetization, magnetic anisotropy, and magnetic phases still mandates further inquiry.

Our aim is to enhance the knowledge of these materials in order to enable the production of layered structures with a more versatile range of tunable magnetic properties. One way to control the magnetic properties in these materials is through the introduction of a third element into the crystal matrix. When a small amount of Rh is added to replace Pt in the equiatomic alloy, new magnetic phases emerge. Exploring the details of the transitions between these phases may enable us to understand better and eventually control the type of magnetic behavior exhibited by the material. Since changing the composition by only a few percent produces different magnetic phases, a superlattice consisting of alternating ferromagnetic and antiferromagnetic layers can be fabricated simply by modulating Rh flux during thin film deposition. We have specifically designed the superlattices under study to have a chemical period accessible with polarized neutron reflectivity, allowing us to probe depth-dependent magnetic order. The detailed magnetic structure of this new class of materials is unknown, since suppressing the changes in lattice constant induced by magnetic phase may occur.

Our initial experiments have confirmed that our superlattices have a strong magnetic modulation with period corresponding to the chemical modulation. The first sample under study was an 8-period superlattice of 25% and 5% FePtRh: [10 nm $Fe_{50}Pt_{45}Rh_5$ / 20 nm $Fe_{50}Pt_{25}Rh_{25}]_8$. We performed extensive characterizations of single-layer $Fe_{50}Pt_{50-x}Rh_x$ films and these investigation resulted in the development of a refined model of the magnetic structures in these alloys. The 5% Rh alloy films are ferromagnetic (FM), and the 25% Rh alloy films are antiferromagnetic (AF) with a spin ordering transition that occurs near 250 K, as verified by neutron diffraction at HFIR, in-house magnetometry, and polarized neutron reflectometry at SNS. For neutron reflectivity it is desirable to use sapphire substrates. The choice of 20 nm as the AF film thickness insures that the it is thicker than a domain wall width, while for the FM, the thickness is chosen such that the change in magnetic anisotropy will create a significant increase in coercivity.

The $\frac{2\pi}{a}(00\frac{1}{2})$ antiferromagnetic Bragg intensity for the $Fe_{50}Pt_{25}Rh_{25}$ film showed a maximum at $T = 275$ K which corresponds to a measured anomaly in the bulk susceptibility. This indicates that different spin ordering vectors are present at low temperature, meaning that the spin structure more complex than the FM sheets with opposite orientations.

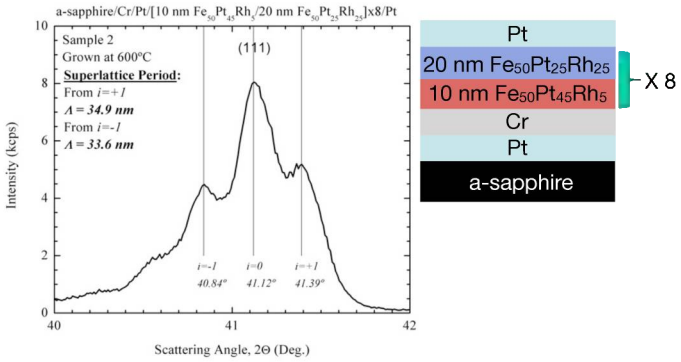

Figure 10: X-ray diffraction results showing the superlattice fringes of the (111) peak as multiple diffraction peaks. This indicates that the chemical order has been modulated, with excellent crystalline quality throughout the superlattice.

1.3.2 Results

That chemically-modulated superlattices can be grown virtually strain-free and has excellent crystal quality is evidenced by our X-ray diffraction results in Fig. 10. The superlattice fringes of the (111) peak as multiple diffraction peaks indicates that the chemical order has been modulated, with excellent crystalline quality throughout the superlattice. The magnetic modulation is evident from polarized neutron reflectivity performed at SNS, Fig. 11, confirming that the magnetic properties are modulated on a length scale of $\sim$30 nm, consistent with the chemical modulation period. Neutron scattering density has both a chemical and magnetic contribution, and the magnetic contribution can be positive or negative, depending on the relative orientations of neutron spin and sample magnetization. In polarized neutron reflectivity measurement, the polarization of the neutrons is flipped relative to the magnetization of the sample and the observed difference in the critical edges is a direct measure of the magnetization of the sample. The peaks in the spectra correspond therefore to Bragg peaks from both chemical and magnetic periodicity. Both R^{++} and R^{--} spectra exhibit Bragg peaks; the much stronger intensity for the R^{++} spectra indicate that the purely *magnetic* periodicity is predominantly responsible for Bragg peaks.

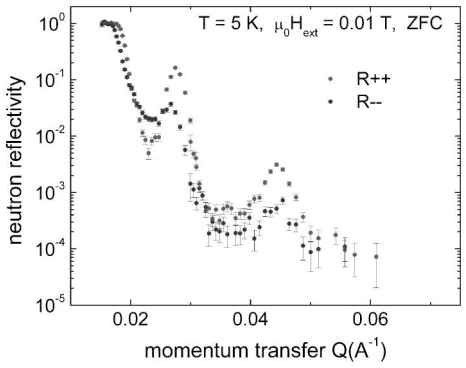

Figure 11: Polarized neutron reflectometry on the superlattice sample, showing reflectivities for neutron spin parallel (R^{++}) and antiparallel (R^{--}) to the applied magnetic field. The change in Bragg peak intensity between R^{++} and R^{--} curves indicate that the magnetic order is modulated on a length scale of $\sim$30 nm, consistent with the superlattice's chemical period.

High-resolution transmission electron microscopy was used to verify the quality of the superlattices and provide local structural information. Figure 12 shows a HAADF-STEM image from

a cross sectional plane of $Al_2O_3(11\bar{2}0)$/Cr/Pt/ $[Fe_{50}Pt_{45}Rh_5$ (10 nm)/$Fe_{50}Pt_{25}Rh_{25}$ (20 nm)$]_8$/Pt multilayer sample. Since the imaging contrast is proportional to Z^2 (Z: atomic weight), the brightly and darkly imaged layers are attributed to the $Fe_{50}Pt_{45}Rh_5$ and $Fe_{50}Pt_{45}Rh_{25}$ (20 nm) layer, and the actual layer thickness is consistent with the expected layer thickness. Furthermore, this result is consistent with an observation of clear satellite peaks in a typical XRD pattern.

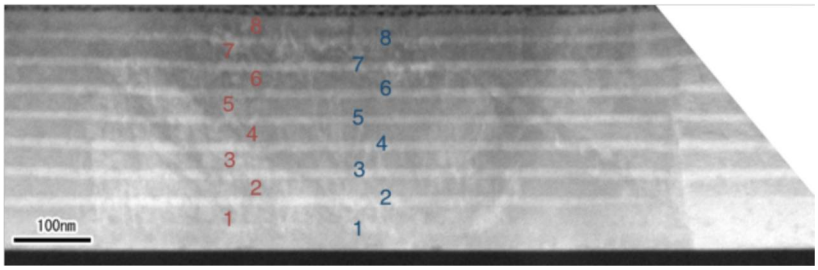

Figure 12: STEM image for $Fe_{50}Pt_{45}Rh_5/Fe_{50}Rh_{25}Pt_{25}$ superlattice sample.

The bright field image for the same sample is shown in Fig. 13 (a). As indicated by arrows, darkly imaging contrast can be observed indicating that the each layer is not a single crystalline one. Figure 13 (b) and (c) show selected area diffraction (SAD) patterns obtained from region I and II in Fig. 13 (a). These SAD patterns are indexed as face-centered-tetragonal phase from the zone axis of [101], and show the [111] direction is orientated along film normal direction. These SAD patterns, Fig. 13 (a) and (b) are rotating 180° each other. This implies that the film was grown with two different stacking sequences, one is ABCABC, and another is CBACBA along film growth direction which resulted in the difference of the electron diffraction patterns.

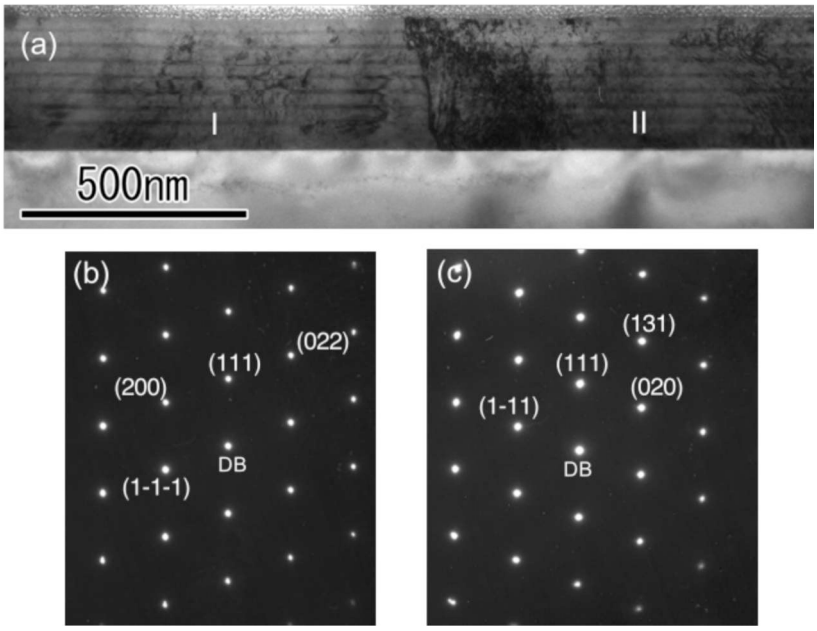

Figure 13: (a) Bright field image for for $Fe_{50}Pt_{45}Rh_5/Fe_{50}Rh_{25}Pt_{25}$ superlattice sample. (b) Electron diffraction pattern obtained in region-I, (b) electron diffraction pattern obtained in region-II.

1.4 Controlling Magnetic Anisotropy in Epitaxial FePt(001) Films

1.4.1 Background

In the past decade, with introduction of new technologies, the areal density of magnetic recording has increased to the point that it exceeds 100 Gb/in^2. To further increase the areal density, it will be necessary to store the data on ferromagnetic particles with scale smaller than $\sim$10 nm. However, for any ferromagnetic material, there is a minimum the grain size necessary to keep an acceptable thermal stability, which is the so-called superparamagnetic limit. To decrease the critical grain size, magnetic materials with high uniaxial anisotropy should be used for recording media. Due to the extremely high uniaxial magnetic anisotropy ($K_u \sim 7 \times 10^7$ erg/cc)[30], the $L1_0$ phase equiatomic FePt alloy is one of the most promising candidates for ultrahigh density magnetic recording.[31]

There is an accompanying writability problem associated with materials with high anisotropy. Since the coercivity of the recording media is roughly proportional to K_u, the ultrahigh K_u of the media material may make it impossible to write on the media with the maximum attainable write head field. An important technical challenge for enabling these concepts is developing an ability to control the magnetic anisotropy of each magnetic layer. In this work by studying dependence of the magnetic properties of epitaxial FePt films on the chemical order parameter S and composition, it is demonstrated that the magnetic anisotropy can be tuned, either by controlling the order parameter or by varying the composition of the alloy thin films.

1.4.2 Results

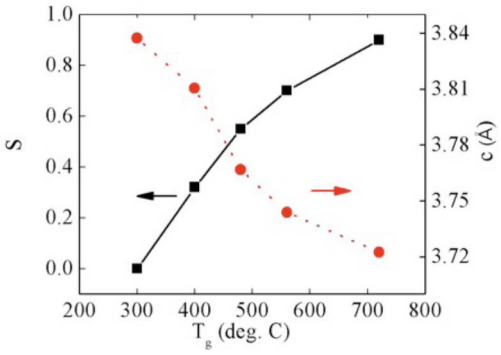

Figure 14: Dependence of order parameter S and lattice constant c on substrate temperature.

$Fe_{100-x}Pt_x$ films with x ranging from 50 to 33 were deposited by DC sputtering from an equiatomic $Fe_{50}Pt_{50}$ alloy target onto single crystalline MgO (001) substrates with Cr (4nm) and Pt (12nm) as buffer layer and seed layers, respectively. Samples were made with $Fe_{50}Pt_{50}$ thin films deposited at various growth temperatures, T_g, ranging from $300-720$°C. The crystal structure of the films was investigated by x-ray diffraction and the magnetic properties of the films were characterized using an alternating gradient magnetometer (AGM).

Our initial investigations show that the order parameter S and lattice constant c as determined by x-ray diffraction depend strongly and monotomically on growth temperature, T_g, as shown in Fig. 14. With the increase of T_g, the order parameter increases: at 300°C, the film is chemically-disordered, while at 750° the film displays nearly perfect chemical order. The maximum growth temperature of 750°C was a limit imposed by the sample heater in the deposition system. It is possible that the films may undergo an order-disorder tran-

sition at even higher temperatures, which would be accompanied by a decrease in chemical order parameter. The c-axis lattice parameter is reduced as the $Fe_{50}Pt_{50}$ transforms from the chemically-disordered fcc phase to the chemicallyordered $L1_0$ phase. Our recent publication tracked the changes in magnetic properties as a function of the order parameter.

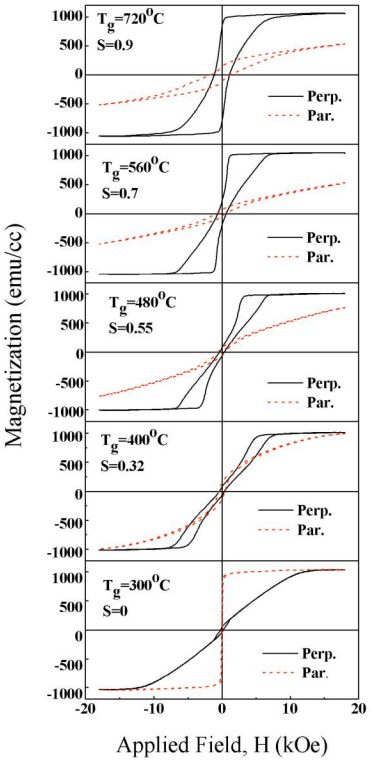

Figure 15: Hysteresis loops for $Fe_{50}Pt_{50}$ films with different order parameter S.

The magnetic properties clearly change as the order parameter S changes, as evidenced by the easy and hard axis loops shown in Fig. 15. The saturation magnetization of all the films is near $1100 \pm 100\,\mathrm{emu/cc}$, which coincides with the value of bulk $L1_0$ $Fe_{50}Pt_{50}$,[32] indicating that changes in the order parameter do not alter the overall magnetization. The films with $S > 0.3$ have out-of plane easy axis, indicated by the bow-type easy-axis loops, suggesting that domain wall motion is involved in the switching.

The hard axis loop of these films has a small coercivity which is likely to be caused by the mixture of ordered and disordered phases. By comparing the hard axis loops of the films with $S > 0.3$, we find that with the increase of S, the hard axis loops requires a larger applied magnetic field to saturate. We can *estimate* H_k, even though the loops are not saturated, by extrapolating the hard axis loop. From the estimated H_k values, we can further calculate the anisotropy taking into account demagnetization, which yields for films with $S = \{0.9, 0.7, 0.5, 0.32\}$ anisotropies of $K_u = \{4.6, 3.3, 2.2, 1.7\} \times 10^7\,\mathrm{erg/cc}$, respectively. In short, a decreasing chemical order parameter leads to a decrease in anisotropy, ranging from a soft in-plane magnetized film to a hard out-of-plane magnetized film. For the application of multilayer exchanged composite media and anisotropy graded media, it is desirable for the material of each layer to have perpendicular anisotropy. According to the results shown above, $Fe_{50}Pt_{50}$ films with S down to 0.32 are sufficient for this application.

1.5 Structural and Magnetic Properties of Epitaxial $Fe_{25}Pt_{75}$

1.5.1 Background

The goal of this work is to learn to control magnetic ordering on the nanoscale. This can be accomplished by studying thin film layers of $FePt_3$ ($Fe_{25}Pt_{75}$), a material which has the remarkable property that, depending on the degree of chemical order, a ferromagnetic (FM) and an antiferromagnetic (AF) magnetic state can coexist at the same temperature. Chemically-ordered epitaxial $FePt_3$ films have two distinct antiferromagnetic phases at temperatures below $\sim 160\,\mathrm{K}$, and exhibit paramagnetism above that temperature. In sharp contrast, chemically-disordered epitaxial $FePt_3$ films are ferromagnetic with a Curie temperature that is greater than $400\,\mathrm{K}$.

The crystal structure of $FePt_3$ is similar to Cu_3Au which is a prototype for a chemical order-disorder transition. Stoichiometric $FePt_3$ in perfectly chemically ordered face-centered cubic (fcc) $L1_2$ structure shows antiferromagnetic order below $T_N = 170\,\mathrm{K}$. In this structure, the chemical order corresponds to the Fe atoms occupying the corners and Pt atoms located at the faces of the cubic cell. The Fe moments ($m_{Fe} = 3.3\,\mu_B$ extrapolated to $T = 0\,\mathrm{K}$) order on (110) alternating ferromagnetic subsheets, while the Pt atoms carry a small moment ($m_{Pt} < 0.2\,\mu_B$). The AF ordered magnetic phase of $FePt_3$ is very sensitive to plastic deformation resulting in chemical disorder [6,7]. Plastic deformation with consequential increased dislocation densities, can be obtained by cold working the chemically ordered alloy, which, in turn, leads to Fe atoms occupying face centered positions rather than corner positions in the fcc ordered lattice [8]. As a result, the positive exchange between next neighbor Fe atoms introduces a tendency to FM order. Completely disordered $FePt_3$ has an fcc structure in which each lattice site is occupied by, on average, $\frac{1}{4}$ Fe and $\frac{3}{4}$ Pt atoms, where the atomic fractions represent probabilities. Chemically disordered bulk FePt orders FM at temperatures below about 425 K.

In this experiment, we aim to demonstrated that by varying the substrate temperature during growth, epitaxial films with varying degrees of chemical order can be produced, and it is possible to produce an alloy with the same composition throughout the film with a modified magnetic structure. To this end, we have used polarized neutron reflectivity to gauge the depth-dependent magnetism of a $Fe_{25}Pt_{75}$ sample produced with a periodic variation in the growth temperature.

1.5.2 Results

In our preliminary work, we demonstrated that the chemical ordering of epitaxial films can be controlled by varying the substrate temperature during growth. In the case of $FePt_3$ grown epitaxially on MgO(001) substrates, we have been able to obtain near perfect chemical ordering for a substrate growth temperature of $600 - 700°\mathrm{C}$, corresponding to the AF $FePt_3$ phase, while the chemical order is essentially absent for growth temperatures of $\sim 400°\mathrm{C}$, corresponding to the FM phase. Thus, by rapidly varying the substrate temperature from 400-700°C during growth, we can produce a superlattice that is chemically homogeneous - as viewed by, e.g., x-ray reflectivity - while displaying a modulation of magnetic order - as viewed by, e.g., polarized neutron reflectivity.

To perform neutron reflectivity measurements, it is desirable to have a periodic variation of the film structure with a few repeats. The repeat periodicity must correspond to the inverse of the momentum transfer range of the instrument to enable the observation of Bragg peaks in the reflectivity data. We chose to fabricate a five period superlattice for this purpose, consisting five bilayers *nominally* of [20 nm $FePt_3$ grown at 600°C (ordered) / 10 nm $FePt_3$ grown at 400°C (disordered)].

From x-ray diffraction data on this sample, we calculate an order parameter for the entire superlattice of $S = 0.56$, corresponding to a thickness-weighted average of the disordered ($S = 0$) and ordered ($S \sim 1$) regions. For this sample, the temperature change was programmed such that the transition region extended into the high- and low-temperature deposited regions. In addition,

it takes about twice as much time to cool down as it does to heat up the sample. The calculated order parameter is consistent with a film consisting of repeats of the following actual structure of $FePt_3$ layers: [15 nm at 600°C / 5 nm cooling from 600-400°C / 7 nm at 400°C / 3 nm heating from 400-600°C].

Figure 16 shows polarized neutron reflectivity measurements of a representative sample at low temperature and room temperature. The critical edge, defined as the momentum transfer at the point where the reflectivity drops to 0.5, is a direct measure of the neutron scattering density of the material. As mentioned above, in polarized neutron reflectivity measurement, the polarization of the neutrons is flipped relative to the magnetization of the sample and the observed difference in the critical edges is a direct measure of the magnetization of the sample. At 300 K, the splitting is nearly zero corresponding to a small residual magnetization of the sample near the Curie temperature. When the sample is cooled to 5 K, the larger magnetic splitting indicates that the sample has a ferromagnetic component which can be correlated with the ferromagnetism of the disordered component of the sample.

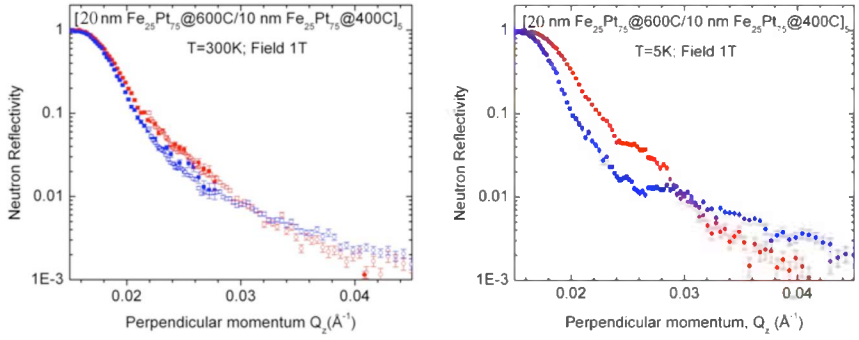

Figure 16: Polarized Neutron Reflectivity of an order-parameter-modulated magnetic superlattice showing the increase in magnetic splitting as the sample is cooled. The red and blue curves are reflectivities for neutron spin parallel (R^{++}) and antiparallel (R^{--}) to the applied magnetic field.

These results indicate that we have produced a superlattice of ordered/disordered $FePt_3$ and verified that the magnetic structure is modulated on the scale of 30 nm using polarized neutron reflectometry. Two features in the temperature dependent reflectivity curves confirm our hypothesis. First, the magnetic splitting, which is the difference between the red and blue curves in Fig. 16 increases dramatically as the sample is cooled below room temperature to 5 K. This indicates the presence of ferromagnetic $FePt_3$ for the component grown at low temperature. Second, the Bragg peak (seen as a hump in the red curve around $Q_z = 0.025\,\text{Å}^{-1}$ at 5 K) appears when the sample is cooled. This indicates a modulation of the magnetic structure on the appropriate length scale. The splitting drops dramatically near room temperature, which is consistent with a ferromagnetic Curie temperature of $360-425$ K for bulk alloys.[33] A reduced Curie temperature of 255 K has recently been observed in $Fe_{25}Pt_{75}$ nanocubes produced by chemical synthesis methods.[34] Further measurements are underway to correlate these observations with magnetometry measurements, which show that the material develops a magnetic exchange bias when it is cooled below the Néel temperature of the antiferromagnetic phase.

2 Publications

2.1 Journal Publications

1. H. Sato, G.J. Mankey, P. LeClair, and O. Myrasov, *Magnetic transition behavior in Fe-Rh-Pd films deposited at various substrate temperatures*, to be submitted

2. S.P. Bennett, H. Ambaye, H. Lee, **P. LeClair**, G.J. Mankey, and V. Lauter, *Direct evidence of anomalous interfacial magnetization in metamagnetic Pd-doped FeRh thin films*, Scientific Reports **5**, 9142 (2015)

3. J. Yu, **P.R. LeClair**, G.J. Mankey, J.L. Robertson, M.L. Crow, and W. Tian, *Exploring the magnetic phase diagram of dysprosium with neutron diffraction*, Phys. Rev. B, **91**, 014404 (2015)

4. T. Saerbeck, F. Klose, D. Lott, G.J. Mankey, Z. Lu, **P.R. LeClair**, W. Schmidt, A.P.J. Stampfl, S. Danilkin, M. Yethiraj, and A. Schreyer, *Artificially modulated chemical order in thin films: A different approach to create ferro/antiferromagnetic interfaces*, Phys. Rev. B. **82**, 134409 (2010)

5. Z. Lu, M.J. Walock, P. LeClair, W.H. Butler, and G.J. Mankey *Controlling Magnetic Anisotropy in Epitaxial FePt(001) Films*, J. Vac. Sci. Tech. **27**, 1067 (2009)

6. Z. Lu, M.J. Walock, P.R. LeClair, G.J. Mankey, P. Mani, D. Lott, F. Klose, H. Ambaye, V. Lauter, M. Wolff, A. Schreyer, H.M. Christen, B.C. Sales, *Structural and Magnetic Properties of Epitaxial* $Fe_{75}Pt_{25}$, J. Vac. Sci. Tech. A, **27**, 770 (2009)

2.2 Conference Talks & Posters

1. Jian Yu, Hideo Sato, Gary J. Mankey, Patrick R. LeClair, J. Lee Robertson and Randy Fishman, *Growth of Dy/Y Superlattices by Sputtering and Characterization by X-ray Diffraction*, American Vacuum Society Conference 2010, Albuquerque, NM

2. H. Sato, J. Yu, G. Mankey, O. Myrasov, P. LeClair, *The order parameter dependence of transition temperature in FeRhPd alloy films*, American Physical Society meeting 2010, Portland OR

3. G. Mankey, *Neutron reflectometry of FePtRh*, International Conference on Neutron Scattering 2010, Knoxville, TN

4. Patrick R. LeClair, Gary J. Mankey, Micheal J. Walock, Hailemariam Ambaye, Valeria Lauter, *Polarized Neutron Reflectivity of Spin Structures in Novel Magnetic Films*, International Conference on Neutron Scattering 2009, May 3 - 7, Knoxville, Tennessee (poster)

5. Thomas Saerbeck, Dieter Lott, Gary J. Mankey, Zhihong Lu, Patrick R. LeClair, and Frank Klose *Enhanced Magnetic Exchange Bias in Epitaxial $FePt_3$ Multilayers Induced by Local Chemical Ordering*, International Conference on Neutron Scattering 2009, May 3 - 7, Knoxville, Tennessee (poster)

6. Michael James Walock, Haile Ambaye, Valeria Lauter, Patrick LeClair and Gary J. Mankey *Interfacial Interactions of FeCo/Ru and FeCo/Pd Multilayers*, International Conference on Neutron Scattering 2009, May 3 - 7, Knoxville, Tennessee (poster)

7. Zhihong Lu, Gary J. Mankey, Michael James Walock, Patrick R. LeClair, *Polarized Neutron Reflectivity Study of Multiphase Epitaxial $Fe_{25}Pt_{75}$*, International Conference on Neutron Scattering 2009, May 3 - 7, Knoxville, Tennessee (poster)

8. Z. Lu, M.J. Walock, P. LeClair, W.H. Bulter, G.J. Mankey, *Controlling Magnetic Anisotopy in Epitaxial FePt(100) Films*, American Vacuum Society 55th International Symposium & Exhibition, Boston, MA Oct. 19-24, 2008 (Talk)

9. M.J. Walock, H., Ambaye, G.J. Mankey, *Interfacial Interactions of Magnetic and Nonmagnetic Spacer Layers in FeCo/Pd and FeCo/Ru Multilayer Stacks*, American Vacuum Society 55th International Symposium & Exhibition, Boston, MA Oct. 19-24, 2008 (Talk)

10. G.J. Mankey, P. Mani, D. Lott, F. Klose, H. Ambaye, M. Wolff, A. Schreyer, H.M. Christen, B.C. Sales, M.J. Walock, Z. Lu, P. LeClair, *Magnetic Exchange Bias in Epitaxial $Fe_{25}Pt_{75}$*, American Vacuum Society 55th International Symposium & Exhibition, Boston, MA Oct. 19-24, 2008 (Talk)

11. Patrick LeClair, Gary J. Mankey, James G. Tobin, *Exchange Interactions in Epitaxial Intermetallic Layered Systems*, DOE-EPSCoR program review 2008, July 22-24, Oak Ridge National Laboratory (poster)

2.3 Beamtime Proposals

1. PLATYPUS instrument proposal, *Spin ordering and exchange bias based on chemical ordering in novel magnetic films,* Thomas Saerbeck (active)

2. ILL-CRG/SNS research proposal, *Magnetic interactions in $Fe_{50}Pt_{50-x}Rh_x$/ $Fe_{50}Pt_{50-x}Rh_x$ bilayer systems,* Dieter Lott, Jochen Fenske, Andreas Schreyer, Gary J. Mankey (active)

3. NSLS research proposal, *Magnetic Xray Reflectivity of Novel Intermetallic Layered Structures,* Gary J. Mankey, Patrick R. LeClair (submitted)

4. SRC research proposal, *X-Ray Magnetic Circular Dichroism of Novel Spintronic Materials,* Patrick R. LeClair, Gary J. Mankey (completed)

3 Participants

	Position	**Facility**	**Demographic**	**Support**
Patrick R. LeClair	PI	UA	US citizen, male	full[†]
Gary J. Mankey	co-PI	UA	US citizen, male	full[1]
Hideo Sato	postdoctoral fellow	UA	Japanese, male	full
Jian Yu	graduate assistant	UA	Chinese, male	none
Valeria Lauter	collaborator	ORNL/SNS[2]	Russian, female	none
Hailemariam Ambaye	collaborator	ORNL/SNS[2]	Somalian, male	none
Lee Robertson	collaborator	ORNL/HFIR[3]	US citizen, male	none
James Tobin	collaborator	LLNL[4]	US citizen, male	none
Frank Klose	collaborator	ANSTO[5]	German, male	none
Dieter Lott	collaborator	GKSS[6]	German, male	none

[1] One month of (summer) salary per year was committed to P. LeClair and G. Mankey.

[2] Oak Ridge National Laboratory / Spallation Neutron Source

[3] Oak Ridge National Laboratory / High Flux Isotope Reactor

[4] Lawrence Livermore National Laboratory

[5] Australian Nuclear Science and Technology Organisation

[6] GKSS research center, *Gesellschaft zur Förderung der Kernenergie in Schiffbau und Schiffstechnik* (society for the promotion of the nuclear energy in shipbuilding and naval technology)

4 Current and Pending Support

4.1 Patrick R. LeClair, PI

Project: Exchange Interactions in Epitaxial Intermetallic Layered Systems
Source of Support: US DOE/EPSCOR
Status: Current
Total Award Amount: $495,000 (incl. $45,000 UA cost share)
Total Award Period Covered: 06/15/08-06/14/11
Location of Project: University of Alabama
Person-Months Per Year Committed to Project: 1.0 Summer

Project: FRG: Rutile heterostructures for spin electronics
Source of Support: NSF
Status: Current
Total Award Amount: $ 563,586
Total Award Period Covered: 08/15/07-08/14/10
Location of Project: University of Alabama
Person-Months Per Year Committed to Project: 1.0 Summer
Overlap with existing DOE-supported project: This project deals specifically with devices based on the Rutile oxides (e.g., TiO_2, CrO_2, etc.). There is no significant overlap, beyond the fact that similar experimental techniques are used in this project.

Project: MRI: A Hybrid Deposition System for Materials Science Research and Education
Source of Support: NSF
Status: Current
Total Award Amount: $413,000 (excl. $177,000 UA cost share)
Total Award Period Covered: 09/01/08-08/30/10
Location of Project: University of Alabama
Person-Months Per Year Committed to Project: 0.0
Overlap with existing DOE-supported project: This is an instrument acquisition project, with no clear relevance to the current DOE-supported project.

Project: NSF-NRI: Spintronic Logic Devices
Source of Support: NSF
Status: Current
Total Award Amount: $324,000
Total Award Period Covered: 09/01/09-08/30/12
Location of Project: University of Alabama
Person-Months Per Year Committed to Project: 0.0
Overlap with existing DOE-supported project: This project deals with devices based on

ultrathin magnetic oxides, specifically insulating ferromagnets. Though the experience gained in advanced magnetic characterization through the DOE-supported project will be invaluable, there is no clear overlap in research topics.

4.2 Gary J. Mankey, co-PI

Project: Exchange Interactions in Epitaxial Intermetallic Layered Systems
Source of Support: US DOE/EPSCOR
Status: Current
Total Award Amount: $495,000 (incl. $45,000 UA cost share)
Total Award Period Covered: 06/15/08-06/14/11
Location of Project: University of Alabama
Person-Months Per Year Committed to Project: 1.0 Summer

Project: MRI: A Hybrid Deposition System for Materials Science Research and Education
Source of Support: NSF
Status: Current
Total Award Amount: $413,000 (excl. $177,000 UA cost share)
Total Award Period Covered: 09/01/08-08/30/10
Location of Project: University of Alabama
Person-Months Per Year Committed to Project: 1.0
Overlap with existing DOE-supported project: This is an instrument acquisition project, with no clear relevance to the current DOE-supported project.

References

[1] M. Fallot *Ann. Phys.*, vol. 10, p. 291, 1938.

[2] M. Fallot and R. Horcart *Rev. Sci.*, vol. 77, p. 498, 1939.

[3] N. V. Baranov and E. A. Baranove *J. Alloys Compd.*, vol. 219, p. 139, 1995.

[4] J. S. Kouvel *J. Appl. Phys.*, vol. 37, pp. 1257–1258, 1966.

[5] P. H. L. Walter *J. Appl. Phys.*, vol. 33, p. 938, 1964.

[6] J. Cao, N. T. Nam, S. Inoue, H. Ko, N. N. Phuoc, and T. Suzuki *J. Appl. Phys.*, vol. 103, p. 07F501, 2008.

[7] J.-U. Thiele, S. Maat, and E. E. Fullerton *Appl. Phys. Lett.*, vol. 82, p. 2859, 2003.

[8] J.-U. Thiele, S. Maat, E. E. Fullerton, and J. L. Robertson *IEEE Trans. Magn.*, vol. 40, p. 2537, 2004.

[9] K. Y. Guslienko, O. Chubykalo-Fesenko, O. Mryasov, R. Chantrell, and D. Weller *Phys. Rev. B*, vol. 70, p. 104405, 2004.

[10] S. Maat, J.-U. Thiele, and E. E. Fullerton *Phys. Rev. B*, vol. 72, p. 214432, 2005.

[11] B. E. Warren, *X-Ray Diffraction.* Reading, Ma: Addison-Wesley, 1969.

[12] M. U. Cohen *Rev. Sci. Instr.*, vol. 6, p. 68, 1935.

[13] M. U. Cohen *Rev. Sci. Instr.*, vol. 7, p. 155, 1936.

[14] J. B. Nelson and D. P. Riley *Proc. Phys. Soc. London*, vol. 57, p. 126, 1945.

[15] A. Zakharov, A. M. Kadomtseva, R. Z. Levitin, and E. G. Ponyatovskii *Zh. Eksp. Teor. Fiz.*, vol. 46, p. 2003, 1964.

[16] L. Zsoldos *Phys. Status Solidi*, vol. 20, p. K25, 1967.

[17] H. Sato, G. J. Mankey, P. LeClair, and O. N. Mryasov. to be submitted.

[18] D. R. Behrendt, S. Legvold, and F. H. Spedding, "Magnetic properties of dysprosium single crystals," *Phys. Rev.*, vol. 109, pp. 1544–1547, 1958.

[19] B. R. Cooper, "Magnetoelastic effects and the magnetic properties of rare-earth metals," *Phys. Rev. Lett.*, vol. 19, pp. 900–903, 1967.

[20] J. Haraldsen and R. Fishman *J. Phys.: Condens. Matter*, vol. 22, p. 186002, 2010.

[21] C. Majkrzak, J. Kwo, M. Hong, Y. Yafet, D. Gibbs, C. Chien, and J. Bohr *Advances in Physics*, vol. 40, p. 99, 1991.

[22] M. Hong, S. Wolf, and D. Gubser, *Metallic Multilayers and Epitaxy.* Warrendale: The Metallurgical Society, 1988.

[23] P. Mangin, C. Dufour, and B. Rodmacq *Physica B*, vol. 192, p. 122, 1993.

[24] C. Majkrzak *Physica B*, vol. 221, p. 342, 1996.

[25] http://som.web.cmu.edu/structures/S058-Al2O3.html.

[26] http://iron.nuc.berkeley.edu/ bdwirth/Public/NE120/documents/Chap2.crystals.pdf.

[27] T. Russell *Mater Sci Rep*, vol. 5, p. 171, 1990.

[28] http://www1.chm.colostate.edu/Files/XRR.pdf.

[29] U. Pietsch, V. Holý, and T. Baumbach, *High-resolution X-ray scattering from thin films to lateral nanostructures.* New York: Springer-Verlag, 2004.

[30] O. Ivanov, L. Solina, V. Demshina, and L. Magat *Phys. Met. Metallogr. (USSR)*, vol. 35, p. 81, 1973.

[31] D. Suess, T. Schrefl, R. Dittrich, M. Kirschner, F. Dorfbauer, G. Hrkac, and J. Fidler *J. Magn. Magn. Mater.*, vol. 290, p. 551, 2005.

[32] O. Ivanov, L. Solina, V. Demshina, and L. Magat *Fiz. Met. Metalloved*, vol. 35, p. 92, 1973.

[33] G. Bacon and J. Crangle *Proc. R. Soc. London, Ser. A*, vol. 272, p. 387, 1963.

[34] O. Margeat, M. Tran, M. Spasova, and M. Farle *Phys. Rev. B*, vol. 75, p. 134410, 2007.